Synthesis and Photophysics of a 1-Pyrenylmethyl-Substituted 2′-Deoxyuridine-5-Carboxamide Nucleoside: Electron-Transfer Product Lifetimes and Energies

Charles E. Kerr,[†] C. Denise Mitchell,[†] Yun-Ming Ying,[†,‡] Bruce E. Eaton,*[,§] and Thomas L. Netzel*[,†]

Department of Chemisty, Georgia State University, Atlanta, Georgia 30303-3083, and Department of Chemistry, Washington State University, Pullman, Washington 99164-4630

Received: October 25, 1999; In Final Form: December 9, 1999

This paper presents results of the synthesis and photophysical study of *N*-(1-pyrenylmethyl)-2′-deoxyuridine-5-carboxamide (PMA-dU) and its spectroscopic model *N*-acetyl-1-aminomethylpyrene (PMA-Ac). The goal in these studies is to learn about the intrinsic forward and reverse electron-transfer (ET) processes in the PMA-dU nucleoside as a means of developing pyrenyl-dU nucleosides with ET product lifetimes in the 0.5 ns time range. Absorbance and emission spectra, emission quantum yields, and emission lifetimes are reported for both compounds in three solvents. The data show that the emission yield quenching varies from 75 to 98% in the solvent series THF, MeCN, and MeOH. Pyrenyl $(\pi,\pi^*)^1$ emission quenching is assigned to ET that forms the pyrene$^{\bullet+}$/dU$^{\bullet-}$ product as observed previously in other pyrenyl-dU nucleosides. In contrast to the monoexponential emission decay of PMA-Ac, the emission of PMA-dU at all wavelengths is multiexponential with 4 lifetimes in THF and nearly always with 3 in MeCN and MeOH. The multiexponential decay is likely due to the presence of multiple nucleoside conformers. Importantly, the emission decay for the nucleoside in the 500−550 nm region is assigned to relaxation of the pyrene$^{\bullet+}$/dU$^{\bullet-}$ ET product. The 0.5−4 ns time range contains over 95% of the emission amplitude in this wavelength region for the polar solvents MeCN and MeOH. Thus, the ET product in PMA-dU appears to have the desired long lifetime. Additionally, CIS INDO/S computations of the excited-state properties of 19 conformers of the nucleoside model *N*-(1-pyrenylmethyl)-1-methyluracil-5-carboxamide (PMA-U$_{Me}$) identify two key factors that control the energy of pyrene$^{\bullet+}$/dU$^{\bullet-}$ ET products. One is ease of reduction of the uracil subunit, in turn controlled by variation of the angle between the uracil-C5 carbonyl and the plane of uracil ($R = 0.90$). The other is Coulombic attraction between the pyrenyl cation and uracil anion subunits. The Coulombic and CO/U$_{Me}$ dihedral angle contributions to the energy of the ET_1 state are independent of each other and can operate either in or out of phase with respect to varying energy of the ET_1 state.

Introduction

In recent years a number of measurements of DNA-mediated electron transfer (ET) have been reported, and this work has also been reviewed several times.[1−3] While the understanding of DNA-mediated ET is growing,[4−11] it is still unclear whether the distance dependence of ET in DNA is always strong or can under some circumstances be quite shallow.[12−19] For example, recent cation migration studies by Giese and co-workers[4,5] investigated the distance dependence of cation migration in DNA indirectly from strand-cleavage assays. These studies provide important information concerning the distance dependence of hole tunneling and hole hopping in DNA, reinforcing the need for direct rate measurements of these reactions.

Our approach to studying charge migration in DNA focuses on examining electron migration from a photoproduced 2′-deoxyuridine anion (dU$^{\bullet-}$) to covalently attached electron acceptor sites.[20] These experiments are designed to measure directly the kinetics of electron migration in DNA by means of laser-flash transient absorbance (TA) spectroscopy. To understand structural influences on dU$^{\bullet-}$ photoproduction in DNA, we have synthesized and studied the photophysics of ET in a family of pyrenyl-dU nucleosides.[21,22] Our earlier work in this area showed that indeed photoinduced electron transfer did occur in ≤30 ps to form the pyrene$^{\bullet+}$/dU$^{\bullet-}$ ET product. However, the longest lifetimes observed for this product were 100 ps in acetonitrile (MeCN) and 67 ps in methanol (MeOH).[22]

An important first step in measuring electron motion in DNA requires trapping an excess electron on deoxyuridine long enough to allow it time to travel to other DNA sites. The competing reaction, of course, is back-ET between the photooxidized pyrenyl ligand (pyrene$^{\bullet+}$) and the initially reduced deoxyuridine nucleoside (dU$^{\bullet-}$). One way of accomplishing this is to make the covalent linker that joins the pyrenyl and deoxyuridine subunits the right length and composition. This would allow the photoinduced charge separation event (formation of pyrene$^{\bullet+}$/dU$^{\bullet-}$) to be ca. 99% efficient and the back (or reverse) ET reaction to be slow enough to allow the electron on the reduced deoxyuridine to transfer to other DNA sites. A variation on this theme that is likely to be both feasible and practical would use a secondary electron donor to reduce the

* To whom correspondence should be addressed.
† Georgia State University.
‡ Present address: Department of Chemistry, Rice University, Houston, Texas 77005-1892.
§ Washington State University.

10.1021/jp993776z CCC: $19.00
Published on Web 02/09/2000

SCHEME 1

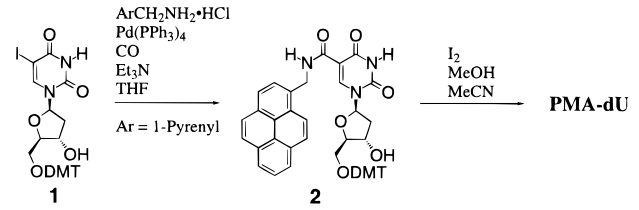

pyrene$^{\bullet+}$ ligand and thus lengthen the lifetime of the trapped dU$^{\bullet-}$ anion.[23]

With these considerations in mind, we present in this paper the results of our synthesis and photophysical study of the 5-(*N*-carboxy-1-aminomethylpyrenyl)-dU nucleoside (PMA-dU). Our immediate goal in these studies is to learn about the intrinsic forward and reverse ET processes in this nucleoside as a means of developing pyrenyl-dU nucleosides with ET product lifetimes in the 0.5 ns time range. Additionally, this paper presents the results of CIS INDO/S computations of the excited-state properties of 19 conformers of a model of this nucleoside, *N*-(1-pyrenylmethyl)-1-methyluracil-5-carboxamide (PMA-U_{Me}). Taken together, these investigations identify two key factors that control the energy of pyrene$^{\bullet+}$/dU$^{\bullet-}$ ET products and show that the ET products in PMA-dU nucleoside conformers are appropriately long-lived.

Materials and Experimental Methods

General Synthetic Methods. Deoxyuridine analogues were prepared by adaptation of previously published procedures.[24] All palladium coupling reactions (Scheme 1) were conducted in a pressure vessel equipped with Teflon stopcocks. A Vacuum Atmospheres, Inc. glovebox (argon or nitrogen atmosphere) was used to store and combine the solvents and reagents for palladium couplings. Reactions conducted outside the glovebox were performed under an argon or nitrogen atmosphere. Tetrahydrofuran (THF) was distilled from benzophenone Na/K alloy and stored with rigorous exclusion of moisture and oxygen. Triethylamine (Et_3N) and acetonitrile (MeCN) were purified by distillation from calcium hydride under an inert atmosphere, and methanol (MeOH) was dried by distillation from magnesium turnings under an inert atmosphere. Whatman silica gel (80 Å pore, 230−400 mesh) and Biotage KP-Sil flash cartridges were used for column chromatography. NMR data were acquired on Bruker and Varian spectrometers (^{1}H, 300 MHz) at the WSU NMRSC and at GSU. Mass spectral data were obtained from facilities at Washington State University and the Georgia Institute of Technology.

Preparation of *N*-(1-Pyrenylmethyl)-5′-*O*-DMT-2′-deoxyuridine-5-carboxamide (2). In an inert atmosphere glovebox, 1-(2′-deoxy-5′-dimethoxytrityl-*β*-D-ribofuranosyl)-5-iodoracil (**1**, 160 mg, 0.244 mmol), 1-(aminomethyl)pyrene hydrochloride (193 mg, 0.721 mmol), tetrakis(triphenylphosphine)palladium-(0) (58 mg, 45.9 μmol), THF (2.4 mL), and Et_3N (0.6 mL) were placed in a Pyrex high-pressure bomb equipped with a Teflon high-vacuum stopcock. The Teflon stopcock was closed and the bomb removed from the box and charged with CO (50 psig). The reaction vessel was then heated in an oil bath (70 °C) for approximately 22 h. The bomb was removed from the bath, allowed to cool, recharged with CO (50 psig), and returned to the oil bath. Heating was continued for another 4 days, after which time the bomb was cooled and the contents collected using MeOH and acetone to wash the bomb. The crude product was concentrated onto flash silica (1 g). Purification was achieved by column chromatography using prepackaged cartridges in a Biotage flash system (KP-Sil 40S) and stepwise elution (1:300 CH_2Cl_2/Et_3N; 500:5:1 CH_2Cl_2/MeOH/Et_3N; 500:10:1 CH_2Cl_2/MeOH/Et_3N; 20:1 CH_2Cl_2/MeOH). Concentration of the appropriate fractions gave **1** (70 mg, 37%) as an oil. This material was used without further purification or to prepare PMA-dU. MS (MALDI) *m*/*z* for $C_{48}H_{41}N_3O_8$•Na $(M + Na)^+$: calcd, 810.279; found, 810.334.

Preparation of *N*-(1-Pyrenylmethyl)-2′-deoxyuridine-5-carboxamide (PMA-dU). Detritylation was performed as described by Ronald and Wahlstrom.[25] **2** (101 mg, 0.128 mmol) was dissolved in MeOH (10 mL) and MeCN (5 mL). The reaction vessel was placed in a 40 °C oil bath and the solution stirred. Iodine (157 mg, 0.619 mmol) was added, and reaction progress was followed thereafter by thin-layer chromatography (TLC) (10% MeOH in CH_2Cl_2, silica). The reaction was quenched after 24 min by addition of aqueous sodium bisulfite (20% w/w, excess) to discharge the iodine color. To the resulting solution, 5 mL of flash silica was added. The mixture was then evaporated under reduced pressure and dried by coevaporation of residual water with MeOH and THF. The dried residue was loaded onto a flash silica column using small volumes of CH_2Cl_2. The product was eluted in a stepwise manner using 2%, 4%, 6%, 8%, and 10% (v/v) mixtures of MeOH in CH_2Cl_2. After in vacuo concentration of the eluate, PMA-dU (55.5 mg, 89.3%) was obtained as an off-white solid. ^{1}H NMR (300 MHz, DMSO-d_6): δ 2.20 (m, 2H, $H_{2'}$), 3.605 (m, 2H, $H_{5'}$), 3.891 (dt, J = 3.3, 3.6 Hz, 1H, $H_{4'}$), 4.265 (m, 1H, $H_{3'}$), 5.072 (t, J = 4.8 Hz, 1H, $OH_{5'}$), 5.256 (d, J = 6.0 Hz, 2H, CH_2 (pyrenyl)), 5.321 (d, J = 3.9 Hz, 1H, $OH_{3'}$), 6.150 (t, J = 6.3 Hz, 1H, $H_{1'}$), 8.086−8.472 (m, 9H), 8.807 (s, 1H, H_6), 9.32 (t, br, J = 5.7, 1H, NH_{amide}), 11.87 (s, br, 1H, H_3). ^{13}C {^{1}H} NMR (75 MHz, DMSO-d_6): δ 40.172, 40.217, 61.186, 70.328, 85.498, 87.833, 105.139, 122.697, 123.781, 123.949, 124.575, 124.918, 125.025, 125.971, 126.360, 126.849, 127.085, 127.505, 127.886, 130.038, 130.092, 130.61, 132.32, 145.918, 149.306, 161.37, 162.995. MS (FAB) *m*/*z* for $C_{27}H_{24}N_3O_6$ $(M + H)^+$: calcd, 486.1666; found, 486.1671.

Preparation of *N*-Acetyl-1-aminomethylpyrene (PMA-Ac). 1-(Aminomethyl)pyrene hydrochloride (625 mg g, 2.33 mmol), pyridine (40 mL), and acetic anhydride (12 mL) were combined and stirred at 50 °C for about 18 h. After in vacuo removal of volatile components, the product was isolated by recrystallization from acetone giving PMA-Ac (467 mg, 73.4%) as an off-white solid that melts with discoloration over the range 203−208 °C (uncorrected) in a Thomas−Hoover melting point apparatus. ^{1}H NMR (300 MHz, DMSO-d_6): δ 1.92 (s, 3H), 4.98 (d, J = 5.6 Hz, 2H), 8.20 (mult, 9H), 8.59 (t, J = 5.6 Hz, 1H). ^{13}C {^{1}H} NMR (75 MHz, DMSO-d_6): δ 18.70, 36.49, 119.13, 119.82, 119.94, 120.618, 121.062, 121.15, 122.16, 122.644, 122.92, 123.28, 123.47, 123.99, 125.98, 126.20, 126.68, 128.90, 164.89. HRMS (EI$^+$) *m*/*z* for $C_{19}H_{15}NO$ (M^+): calcd, 273.1154; found, 273.1155.

UV−Visible Absorbance and Emission Spectroscopic Methods. Absorbance spectra were recorded on a Shimadzu UV 2501PC high-performance spectrophotometer equipped with a double monochromator for reduced stray light. The bandwidth for absorbance spectra was 1 nm, and sample concentrations were $(1.5-3.0) \times 10^{-5}$ M. Molar absorbance coefficients (ϵ) for PMA-dU and PMA-Ac were measured in THF, MeCN, and MeOH. An amount (1.1−1.9 mg) of PMA-dU or PMA-Ac was weighed to ±0.01 mg and dissolved by stirring for 1 week in a 100 mL volumetric flask. Quantitative dilutions were made to produce Beer's law plots for ϵ calculation. However, poor solubility of PMA-Ac and PMA-dU in THF and MeCN made

measurements for these two solvents unreliable. The solubility of these compounds was much better in MeOH, and ϵ values in this solvent are reported below and were used for concentration determinations for all three solvents.

Fluorescence spectra were recorded on an SLM-8000C (SLM Aminco, Inc.) spectrofluorometer and corrected for the spectral response of the optical system. The correction factors were determined at GSU using a standard lamp whose energy output was traceable to NIST calibrations. The corrected emission spectra reported in this paper are plotted as relative detected-intensity versus wavelength. To eliminate nonisotropic emission polarization artifacts for both emission spectra and quantum yield measurements, a quartz achromatic depolarizer was placed in the excitation beam, and the emission was recorded through a calcite polarizer set at 54.7° with respect to vertical.[26] This defined the polarization of the light in the emission detection system and allowed correction factors to be developed. The excitation wavelength for both emission spectra and quantum yield measurements was 341 nm. For emission spectra the excitation and emission bandwidths were 4 nm and sample concentrations were $(2.0-3.0) \times 10^{-6}$ M.

For emission quantum yield measurements (Φ_{em}), the excitation and emission bandwidths were 2 nm and the absorbances of the two samples (unknown and reference) being compared were made nearly identical at 341 nm at an absorbance value close to 0.1. The corrected emission area (integral of corrected emission quanta versus wavelength, D) for each sample and reference solution was then directly measured. Emission quantum yields were calculated according to eq 1.[27]

$$\Phi_{em}^{x} = \Phi_{em}^{r}\left(\frac{D_x\eta_x^2}{A_x}\right)/\left(\frac{D_r\eta_r^2}{A_r}\right) \quad (1)$$

In eq 1 x and r refer to the unknown and reference solutions, respectively, D_x is the corrected emission area of the unknown solution, A_x is the absorbance of the unknown solution at the exciting wavelength, and η_x is the refractive index of the unknown solution.

For reference use the fluorescence quantum yield for deoxygenated 1-pyrenylbutanoic acid (PBA; Molecular Probes, Inc., High Purity Grade) in MeOH (spectroscopic or HPLC grade) was measured to be 0.065(2) relative to 9,10-diphenylanthracene (Aldrich, 98%) in cyclohexane (spectroscopic or HPLC grade, $\Phi_{em} = 1.00$).[28] The emission quantum yields of PMA-Ac and PMA-dU were subsequently measured relative to either deoxygenated or aerated PBA in MeOH (Φ_{em}(aerated) = 0.0045(2)). To remove oxygen, solutions for emission spectra, quantum yield determinations, and emission lifetime measurements were bubbled with solvent-saturated argon. All PMA-Ac and PMA-dU samples were deoxygneated. Samples were contained in four-sided fluorescence cells (1 cm optical path length) equipped with a valve (Teflon-to-glass seal) and a septum-sealed sidearm. Argon gas was introduced via a cannula through the septum and open valve to the bottom of the solution. After the solution was bubbled for 30−45 min with magnetic stirring, the cannula was partially retracted, the valve closed, and the cannula removed from the septum. PBA emission in such a deoxygenated cell decreased because of oxygen diffusion and quenching less than 1% over 1 h. All emission measurements took less than 30 min.

Fluorescence Lifetime Measurements. All fluorescence decays were recorded on a Tektronix SCD1000 transient digitizer (≤0.35 ns rise time calculated from the bandwidth, ≤120 ps rise time for a step input 0.5 times the vertical range), and the wavelength resolved with a 0.1 m double monochromator (Instruments SA, Inc. model DH10) in additive dispersion. Two millimeter slits were used, producing an 8 nm band-pass. The 1200 grooves/mm holographic gratings were blazed at 450 nm. After passing through the monochromator, the emission was detected with a Hamamatsu 1564U microchannel plate (200 ps rise time) for short emission lifetimes or a Hamamatsu 928 photomultiplier (2.2 ns rise time) for long ones. The excitation and emission beams were oriented at 90° with respect to each other. Emission was detected through a Glan−Thompson polarizer set at 54.7° ("magic angle") with respect to vertical to eliminate artifacts due to rotational diffusion.[26] Additionally, emission was excited at 355 nm with the third harmonic of an active−passive mode-locked Nd^{3+}:YAG laser manufactured by Continuum, Inc. Typically, 35 μJ excitation pulses of ca. 25 ps duration were collimated into a 3 mm diameter beam and passed through a second Glan−Thompson polarizer set to vertical before entering the sample cuvette. Sample concentrations were adjusted so that the absorbance at 355 nm was 0.13−0.16 in a 1 cm cell, and solution absorbance spectra were measured before and after lifetime measurements to verify that no decomposition occurred during these measurements. Photon Technology Incorporated software was modified by the manufacturer to process 1000 data points per decay curve and was used to deconvolute the instrument response from the emission decay to yield exponential lifetime fits to the emission decay data.

The temporal resolution of the emission kinetics system for multiexponential emission decays is generally ca. 0.2 ns; however, for nearly single-exponential decays it can be as good as ca. 50 ps after deconvolution.[21,22] A full description of the lifetime fitting procedure used here is presented in a recent paper by Netzel et al.[21] Included there are nine sets of emission decays on four time scales (20, 50, 100, and 500 ns) along with the following information: the equations used; plots of residual differences between experimental emission decays and calculated multiexponential curves; linear and logarithmic plots of emission decays, lamp decays, and exponential curves; and specific χ_r^2 values (the reduced χ^2 statistic) for the plotted curves.

Results

UV−Visible Absorbance and Emission Spectra for PMA-Ac and PMA-dU. Figure 2 presents composite absorbance and emission spectra for both PMA-Ac and PMA-dU in MeOH. Inspection shows that above 300 nm the absorbance and emission spectra of PMA-Ac and PMA-dU are identical to each other. Additionally, the absorbance spectrum of PMA-Ac is identical to that of PBA above 220 nm. The emission spectrum for PMA-Ac differs from that for PBA not in the locations of the origin and vibrational features but modestly in the relative intensity of these features. Thus, the methylene group on PMA-Ac effectively isolates the amide group from electronic communication with the pyrenyl π-system. Below 300 nm the absorbance spectra of PMA-Ac and PMA-dU differ because the nucleoside's spectrum has contributions from electronic transitions on both the pyrenyl and uracil subunits. As solvent is varied in the series MeCN, THF, and MeOH, the absorbance spectra of both PMA-Ac and PMA-dU remain nearly identical to those shown in Figure 2 at all wavelengths with the small difference that in THF all of the vibrational peaks are red-shifted by 2 nm.

The emission spectra for PMA-Ac and PMA-dU in this same solvent series are also quite similar to those shown in Figure 2. The vibrational amplitudes of the emission spectra in THF are nearly identical to those in MeOH but with a 2 nm red shift of

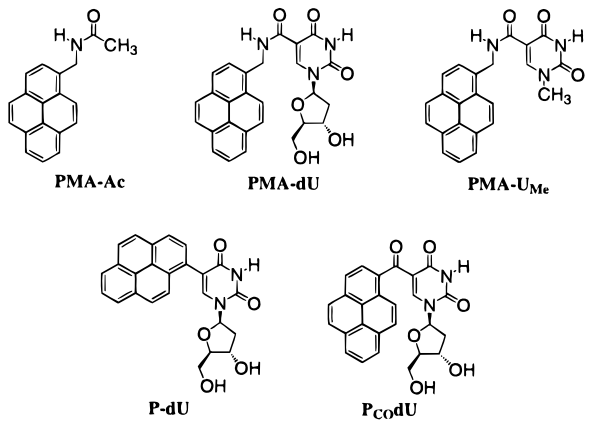

Figure 1. Structural drawings of the pyrenyl spectroscopic model *N*-acetyl-1-aminomethylpyrene (PMA-Ac), *N*-(1-pyrenylmethyl)-2′-deoxyuridine-5-carboxamide (PMA-dU), the computational model *N*-(1-pyrenylmethyl)-1-methyluracil-5-carboxamide (PMA-U_{Me}), and two other pyrene−deoxyuridine nucleosides: 5-(1-pyrenyl)-2′-deoxyuridine (P-dU) and 5-(1-pyrenylcarbonyl)-2′-deoxyuridine (P_{CO}dU).

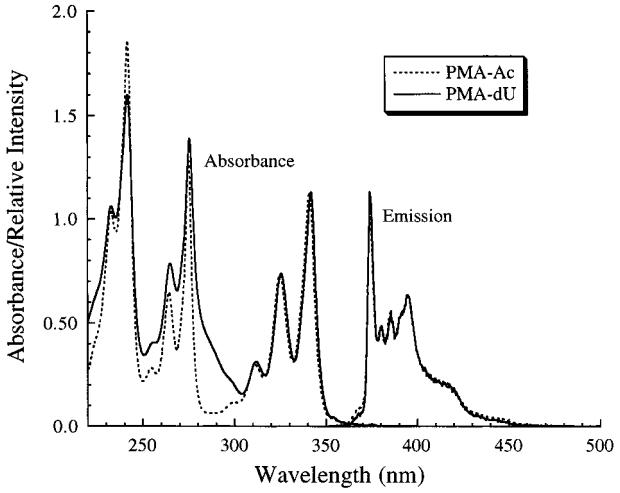

Figure 2. Normalized absorbance and corrected relative emission spectra for PMA-Ac and PMA-dU in MeOH. For absorbance spectra the concentrations were 2.1×10^{-5} and 2.6×10^{-5} M, respectively. For emission spectra the concentrations were both 2.5×10^{-6} M.

their peak positions. The relative vibrational amplitudes for both PMA-Ac and PMA-dU in MeCN are more similar to those of PBA than those shown in Figure 2 for MeOH. However, on balance, the absorbance and emission spectra of both PMA-Ac and PMA-dU are little affected by changes of solvent from nonpolar (THF, static dielectric constant (ϵ_s) = 7.6) to polar nonprotic (MeCN, ϵ_s = 37.5) and to polar protic (MeOH, ϵ_s = 33.6). Interestingly, to the extent pyrene$^{\bullet+}$/dU$^{\bullet-}$ ET states exist in the PMA-dU nucleoside above 375 nm (the electronic origin for the orbitally forbidden $S_0 \rightarrow S_1(\pi,\pi^*)$ pyrenyl absorption, the $(\pi,\pi^*)^1$ state), they either have small molar absorbance coefficients or have significantly altered nuclear positions relative to the ground state. Although the lack of ET product absorbance in the nucleoside above 375 nm indicates weak ground-state electronic interaction between its pyrenyl and uracil subunits, this does not itself guarantee that ET between these subunits will always be nonadiabatic (see discussion below).

The molar absorbance coefficients of PMA-Ac and PMA-dU in MeOH are, respectively, 49 700 (±900) at 341 nm and 43 800 (±300) M^{-1} cm^{-1} at 342 nm. Because the nucleoside is less soluble than PMA-Ac, its slightly lower molar absorbance coefficient for the same electronic transition as in PMA-Ac might be due to incomplete solution. However, its solutions were

TABLE 1: Emission Quantum Yield and Relative Emission Quenching in Three Solvents

compound	solvent	$\Phi_{em} \times 10^3$ [a]	relative quenching,[b] %
PMA-Ac	THF	64(2)	
	MeCN	63(1)	
	MeOH	58(1)	
PMA-dU	THF	16(1)	75(2)
	MeCN	1.1(0.1)	98(1)
	MeOH	5.6(0.6)	90(2)

[a] (±error). Φ_{em} measured relative to deoxygenated PBA in MeOH, $\Phi_{em} = 65(2) \times 10^{-3}$. [b] Relative quenching = $[1 - \Phi_{em}(\text{PMA-dU})/\Phi_{em}(\text{PMA-Ac})] \times 100\%$.

TABLE 2: Emission Lifetimes and Radiative Rates for PMA-Ac and PBA

compound	solvent	τ,[a] ns	$k_{rad} \times 10^{-5}$, s^{-1}
PMA-Ac	THF	254(1)	2.52(0.08)
	MeCN	244(3)	2.59(0.06)
	MeOH	252(2)	2.03(0.06)
PBA	MeOH	219(1)	2.97(0.10)

[a] (±error). Only one emission lifetime (τ) was observed in each solvent, and it was independent of observation wavelength.

stirred for 1 week, and no solid particles were visible either in their interiors or in their menisci. Concentrations of PMA-Ac and PMA-dU in THF and MeCN were determined using the above molar absorbance coefficients for each compound in MeOH.

Emission Quantum Yields for PMA-Ac and PMA-dU. Table 1 lists the emission quantum yields (Φ_{em}) for PMA-Ac and PMA-dU in three solvents and the quenching of emission from the nucleoside relative to emission from PMA-Ac in each solvent. These data show that the emission quenching varies from 75 to 98% in the solvent series THF, MeOH, and MeCN. These substantial fractions of emission quenching are consistent with an intramolecular ET reaction from the pyrenyl $(\pi,\pi^*)^1$ state to form a pyrene$^{\bullet+}$/dU$^{\bullet-}$ ET product. The two polar solvents show more quenching than does less polar THF. It is somewhat surprising that MeCN shows greater quenching than does MeOH, since its dielectric constant (37.5) is only a little larger than that of MeOH (33.6). According to these data, the polar protic solvent MeOH does not increase quenching relative to MeCN, a polar but nonprotic solvent (see additional discussion below).

PMA-Ac Emission Lifetimes. Table 2 lists emission lifetimes (τ) and corresponding radiative rates ($k_{rad} = \Phi_{em}/\tau$) for PMA-Ac in three solvents and for PBA in MeOH. The radiative rate for PMA-Ac is the same in the two nonprotic solvents and 20% smaller in MeOH. Additionally, the radiative rate of PBA in MeOH is distinctly larger than that of PMA-Ac in the same solvent. This radiative rate difference between PBA and PMA-Ac reflects marginally different electronic structures for their lowest energy $(\pi,\pi^*)^1$ states. However, on balance, the single methylene group of PMA-Ac renders it electronically similar to PBA by isolating the pyrenyl and acetylamino chromophores. Note that the long fluorescence lifetimes of PMA-Ac and PBA are a result of the forbidden character of their $S_0 \rightarrow S_1$ absorption processes. The strong absorbance maxima at 341 nm for PMA-Ac and PMA-dU in Figure 2 correspond to the $S_0 \rightarrow S_2(\pi,\pi^*)$ optical transition.

PMA-dU Emission Lifetimes. Figure 2 shows that the $(\pi,\pi^*)^1$ emission from both the pyrenyl subunit of PMA-dU and from PMA-Ac is prominent in the 370−450 nm range and relatively nonexistent above 475 nm. In striking contrast Table 3 reports that under conditions of laser excitation at 355 nm, emission from the PMA-dU nucleoside can be seen in the 500−

TABLE 3: Emission Lifetimes (ns) for PMA-dU in Three Solvents[a]

λ (nm)	375	395	420	450	500	550
THF	0.6 ± 0.1 (26%)	0.8 ± 0.1 (31%)	1.2 ± 0.2 (32%)	1.2 ± 0.1 (41%)	0.5 ± 0.1 (58%)	0.5 ± 0.1 (62%)
	21 ± 4 (21%)	16.9 ± 0.6 (25%)	16 ± 2 (28%)	9.7 ± 0.4 (29%)	4.6 ± 0.1 (30%)	4.3 ± 0.1 (27%)
	48.5 ± 0.2 (52%)	48.9 ± 0.2 (43%)	49.3 ± 0.4 (39%)	52.8 ± 0.4 (29%)	68.3 ± 0.1 (11%)	67.2 ± 0.2 (10%)
	273 ± 7 (1%)	280 ± 4 (1%)	290 ± 18 (1%)	232 ± 16 (1%)	142 ± 20 (1%)	154 ± 7 (1%)
MeCN	0.8 ± 0.2 (14%)	0.7 ± 0.2 (22%)	0.6 ± 0.1 (32%)	0.5 ± 0.1 (58%)	0.5 ± 0.1 (64%)	0.5 ± 0.1 (70%)
	3.0 ± 0.1 (82%)	3.3 ± 0.1 (70%)	3.4 ± 0.1 (60%)	3.6 ± 0.1 (37%)	4.3 ± 0.1 (30%)	4.6 ± 0.3 (26%)
	215 ± 7 (4%)	204 ± 3 (8%)	183 ± 1 (8%)	118 ± 2 (5%)	88 ± 1 (6%)	81 ± 5 (4%)
MeOH	0.5 ± 0.1 (85%)	0.5 ± 0.1 (81%)	0.7 ± 0.1 (74%)	0.8 ± 0.1 (70%)	0.8 ± 0.1 (65%)	0. 8 ± 0.1 (57%)
		8.4 ± 0.8 (7%)	7.2 ± 1.5 (14%)	4.0 ± 0.2 (24%)	4.1 ± 0.1 (33%)	4.1 ± 0.1 (39%)
	202 ± 1 (15%)	198 ± 1 (12%)	192 ± 2 (12%)	152 ± 4 (6%)	69 ± 2 (2%)	66 ± 1 (4%)

[a] Reduced χ_r^2 values for the lifetime fits are in the range 1.6−3.0 for wavelengths 375−420 nm and 1.8−3.7 for 450 nm for all solvents. χ_r^2 values for wavelengths 500−550 nm are 2.6−5.7 for THF and MeCN and 1.8−3.7 for MeOH. The excitation light was a 30 ps laser pulse at 355 nm.

550 nm range in all solvents. Similar long-wavelength emission in other pyrenyl-substituted nucleosides has been reported previously and assigned to emission from a pyrene$^{\bullet+}$/dU$^{\bullet-}$ ET product.[21] Thus, emission kinetics in the 370−420 nm region reflect the quenching of the pyrenyl $(\pi,\pi^*)^1$ state, while emission kinetics at 500 and 550 nm reflect the relaxation dynamics of the pyrene$^{\bullet+}$/dU$^{\bullet-}$ ET product. The 450 nm region appears to have emission kinetics that are intermediate between those of the $(\pi,\pi^*)^1$ and ET regions. In THF the 450 nm kinetics are more similar to the $(\pi,\pi^*)^1$ kinetics than to the ET kinetics, while in MeCN and MeOH the reverse is true.

$(\pi,\pi^*)^1$ Emission Lifetimes in PMA-dU. In contrast to the monoexponential kinetics for $(\pi,\pi^*)^1$ emission from PMA-Ac, the $(\pi,\pi^*)^1$ emission from the PMA-dU nucleoside decays with 4 lifetimes in THF and almost always with 3 in MeCN and MeOH. The multiexponential emission decay is likely due to the presence of multiple nucleoside conformers. (This topic will be discussed again later in this paper.) Whether there are only a few conformers or a broad distribution of conformers with a few principle lifetimes cannot be determined from the data in Table 3. The effect of varying solvent on the $(\pi,\pi^*)^1$ emission kinetics can be judged in several ways. One is to calculate the average emission lifetimes ($\langle\tau\rangle$) in the 375−420 nm range along with their corresponding lifetime quenching values ($[1 - \langle\tau\rangle/\tau_0] \times 100\%$, where τ_0 is the lifetime of PMA-Ac in the same solvent). The average $(\pi,\pi^*)^1$ lifetimes for PMA-dU in THF, MeCN, and MeOH are, respectively, 29(2), 16(4), and 27(2) ns, which correspond to lifetime quenching values of 88(1), 93(2), and 89(1)%. These lifetime quenching values are in reasonable agreement with the emission yield quenching values given in Table 1 of 75, 98, and 90% for the same solvent series. This correspondence of the quenching values for the lifetime and emission yield measurements also provides a check on the emission kinetics fits.

Two other ways of viewing the solvent effects on the $(\pi,\pi^*)^1$ emission lifetimes of PMA-dU can be based on the amplitude variations of the emission decays at 395 nm in the <1 and <4 ns time ranges. It is convenient to use 395 nm data, since it is in the middle of the $(\pi,\pi^*)^1$ emission range. In the <1 ns range, the decay amplitudes are 31, 22, and 81%, respectively, for THF, MeCN, and MeOH, while in the <4 ns range, the amplitudes are 31, 92, and 81%, respectively. Clearly, THF produces a smaller percentage of the fastest quenching conformers than do the more polar solvents MeCN and MeOH. Comparison of quenching kinetics in MeCN and MeOH is more complex. MeOH produces by far the largest fraction of conformers that quench $(\pi,\pi^*)^1$ emission in less than 1 ns (81 versus 31 and 22%, respectively, for THF and MeCN). However, MeCN produces the largest fraction of conformers that quench in less than 4 ns (92 versus 31 and 81%, respectively, for THF and MeOH). Thus, no obvious conclusions can be based on the relative quenching effects in a polar protic solvent versus a polar nonprotic one. These observations of emisson quenching for PMA-dU in MeOH and MeCN contrast with those for P-dU (see Figure 1) in the same solvents.[22] For the P-dU nucleoside, the emission quantum yield increases 13-fold on changing from MeOH to MeCN. Thus, for the P-dU nucleoside a much greater amount of quenching occurs in the polar protic solvent than in the polar nonprotic one.

TABLE 4: ET Product Emission Lifetimes for PMA-dU and P_{CO}dU in MeOH

nucleoside	lifetime, ns	amplitude, %
PMA-dU[a]	0.8 ± 0.1	65
	4.1 ± 0.1	33
	69 ± 2	2
P_{CO}dU[b]	0.4 ± 0.1	68
	1.8 ± 0.1	11
	7.2 ± 2	21

[a] Emission kinetics at 500 nm. [b] Emission kinetics at 495 nm.[21]

ET Product Emission Lifetimes for PMA-dU. The 500 and 550 nm regions in Table 3 provide information on the dynamics of the pyrene$^{\bullet+}$/dU$^{\bullet-}$ ET product. A striking 90−95% of the emission in this region decays in <5 ns in all three solvents. Also, in all three solvents, 5−10% of the emission in this region decays in 65−80 ns, 25−40% of it in 4−5 ns, and 60−70% of it in the 0.5−0.8 ns time range. This pattern of emission lifetimes and amplitudes is both reasonably independent of solvent and different from the corresponding pattern of emission lifetimes found in the 375−420 nm $(\pi,\pi^*)^1$ emission region. The different solvent dependence of the patterns of emission lifetimes in the 500−550 and 375−420 nm regions is in accord with the assignment of different emitting species for these two spectral regions. In MeOH it is clear that the shortest decay components of the 500−550 nm emission (0.8 ns) are longer than the shortest decay components of the 375−395 nm emission (0.5 ns). However, grow-in of the longer wavelength emission from the ET product is not observed.

Comparison of ET Product Emission in PMA-dU and P_{CO}dU. Transient absorbance measurements for P_{CO}dU in MeOH indicated pyrene$^{\bullet+}$/dU$^{\bullet-}$ ET product formation in ≤30 ps. This product decayed with two lifetimes, 67 ps (90%) and 6 ns (10%).[22] The emission decay kinetics listed in Table 4 for this nucleoside are in good agreement with this transient absorbance result, keeping in mind the greater precision and signal-to-noise of the emission kinetics data.[21] Comparing the emission decays at ca. 500 nm in MeOH for PMA-dU and P_{CO}-dU in Table 4 shows that the ET product in the former nucleoside has longer first and second lifetime components (0.8

and 4.1 ns) than it does in the latter nucleoside (0.4 and 1.8 ns). The longest lifetime components possibly reflect slow ET product formation kinetics more than they reflect intrinsic ET product decay kinetics. Also, they comprise only 2−21% of the emission signal. Thus, comparison of the emission decays of these two nucleosides in the 500−550 nm range shows that the pyrene$^{\bullet+}$/dU$^{\bullet-}$ ET product in PMA-dU lives longer than the one found in the P_{CO}dU nucleoside.[29]

Computational Modeling of ET Product Energies in PMA-dU

Computational Modeling Objectives. Comparing the ET product emission lifetimes in PMA-dU to those in P_{CO}dU shows that the lifetime of the pyrene$^{\bullet+}$/dU$^{\bullet-}$ product is longer in the former than in the latter nucleoside. The multiple emission lifetimes evidence multiple PMA-dU conformers during the lifetime of the excited state of pyrene. We thus ask, "What conformers are likely to be present at the time PMA-dU is photoexcited, and what are the relative energies of their pyrene$^{\bullet+}$/dU$^{\bullet-}$ product states?" Answering these questions can give us insight both into the factors that control ET product formation and decay and into the origin of the multiple emission decays discussed above. The remainder of this paper reports the results of our theoretical computations in these two areas. Three objectives of these computations are (1) to gain insight into the important geometries of likely ground-state nucleoside conformers, (2) to estimate the range of variation of their ET product energies, and (3) to understand the factors responsible for these energy variations. Accomplishing these objectives may suggest ways of improving pyrenyl-substituted deoxyuridine designs for use in DNA-mediated electron migration studies.

PMA-U_{Me} Computational Model. To emphasize pyrenyl−uracil interactions as well as to shorten computation times, PMA-dU was modeled as *N*-(1-pyrenylmethyl)-1-methyluracil-5-carboxamide (PMA-U_{Me}; see Figure 1). Both to shorten computation times and to achieve good ground-state geometries, the semiempirical PM3 quantum mechanical method was used for conformational searching.[30,31] Spartan 5.1.1[32] provided a convenient conformational search method based on randomly varying the angles of the four bonds linking pyrene to uracil and storing the resulting minium energy geometries. This search procedure produced 11 conformers with a trans amide bond and 8 with a cis amide bond. [For the following discussion the "amide" term in references to cis amide and trans amide conformers will be dropped; i.e., all cis and trans conformer descriptions will refer to the amide bond.] Note that steric interactions constrain N-monosubstituted acetamides and alkylamides to trans amide conformations (see additional discussion below).[33] Thus, both PA-Ac and PA-dU are expected to be constrained to the trans amides. However, we have only indirect NMR evidence (see below) for this conformational assignment. Thus, computations of ET product energy within the trans family of PA-U_{Me} conformers were also performed to determine whether the energy range spanned by these products was large enough to account for the wide range of quenching lifetimes found for the PMA-dU nucleosides (see Table 3).

Conformer Heat of Formation Energies. The relative heat of formation energies for the 11 trans conformers spanned the 0.000−0.090 eV range [$(0.0-3.6)k_BT$, where k_B is the Boltzmann constant and $T = 298$ K], and the relative heat of formation energies for the 8 cis conformers spanned the 0.095−0.012 eV range [$(3.8-4.8)k_BT$]. As expected, the trans conformers were calculated to be lower in energy than the cis conformers.

Conformer ET Product Energies. The conformer geometries found with Spartan 5.1.1 were transferred to HyperChem 5.1[34] where CIS[35] (configuration interaction with single-excitation determinants) INDO/S[36−38] (intermediate neglect of differential overlap approximate Hamiltonian with spectroscopically adjusted integral parameters) semiempirical computations of excited-state properties were carried out. In this way vertical energies of the excited states (i.e., holding the ground-state geometry constant) were determined. For the CIS computations, 10 HOMO and 10 LUMO orbitals were included. Increasing the number of these orbitals did not affect the energies of the lowest several singlet pyrenyl and ET product states. Note that the INDO/S method has been parametrized to give reasonable agreement with experimental excited-state energies. Since it is possible to use a dielectric continuum solvent model to "solvate" the vertical CIS energies, but it is not possible to geometry-optimize continuum-solvated excited states with available software, vertical energies are preferred for comparison with future studies of the solvent effects on pyrenyl−uracil excited states. Additionally, the vertical excited-state energies are probably sufficient to accomplish the above objectives.

The 11 trans conformers had lowest-energy singlet ET product (ET_1) energies that spanned the 3.94−4.63 eV range, while the corresponding states in the 8 cis conformers spanned the 4.42−4.82 eV range. Thus, the ET excited states tended to be lower in energy for the trans conformers than for the cis ones. It also appears that the range of energies within the trans family of conformers is large enough (ca. 0.7 eV) to be consistent with a wide range of ET quenching rates. It is important to recognize here that the range of energies for local $(\pi,\pi^*)^1$ states arising from the pyrenyl subunit is 3.77−3.83 eV with 18 of the 19 PMA-U_{Me} conformers having $(\pi,\pi^*)^1$ state energies in the 3.77−3.78 eV range. Comparison of the ET and $(\pi,\pi^*)^1$ state energies shows that in the gas-phase all ET quenching reactions in PMA-U_{Me} are endergonic by at least 0.16 eV. However, polar solvents can lower the energy of ET product states more than they lower the energy of local $(\pi,\pi^*)^1$ states. Thus, at least some of the PMA-U_{Me} conformers are expected to have exergonic ET quenching reactions in such solvents. Indeed, preliminary CIS INDO/S results for PMA-U_{Me} in a polar solvent model (spherical solute cavity in a dielectric continuum with a static dielectric constant of 40) confirm the expected differential solvent stabilization of the ET states relative to the local $(\pi,\pi^*)^1$ states for ET states with sufficiently large dipole moments.

Redox Effects on ET State Energies. The *trans*-PMA-U_{Me} conformers can be grouped into three clusters on the basis of their ET_1 state energies: low energy (3.94−4.19 eV), mid-energy (4.30−4.45 eV), and high energy (4.60−4.63 eV). There are four conformers in the low-energy cluster, five in the mid-energy one, and two in the high-energy one. There is no correlation between the heat of formation energies of conformers and their ET_1 state energies. For example, the low-energy cluster has confomers with both the lowest and highest heats of formation. Table 5 presents computational results on five PMA-U_{Me} conformers. The trans conformers **A** and **B** have similar CO/U_{Me} (CO−C5−C6) dihedral angles (12−18°) as do conformers **C** and **D** (41−47°). The cis conformer **E** has a CO/U_{Me} dihedral angle of −87°. Figure 3 presents ball-and-stick models of the trans conformers **A** and **B** and of the cis conformer **E**. Indeed, the CO/U_{Me} dihedral angles of all the trans conformers are in the |12−48|° range, while those of the cis conformers are in the |60−87|° range. Figure 4 is a plot of the uracil subunit's LUMO energy versus the absolute value of the corresponding CO/U_{Me} dihedral angle for all 19 PMA-U_{Me}

TABLE 5: CIS INDO/S Results for Five PMA-U_{Me} Conformers

conformer	amide bond geometry	relative heat of formation (eV)	CO/U_{Me} dihedral angle[a] (deg)	C1−C5 distance[b] (Å)	center-to-center distance[c] (Å)	C7−N1 distance[d] (Å)	$S_1(\pi,\pi^*)$ energy[e] (eV)	$S_1(\pi,\pi^*)$ dipole moment[e] (D)	ET_1 energy[f] (eV)	ET_1 dipole moment[f] (D)	uracil LUMO[g] (eV)
A	trans	0.0000	12.0	4.52	7.72	10.97	3.77	2.53	4.16	28.3	−0.82
B	trans	0.0319	18.1	4.90	8.72	12.66	3.77	2.59	4.45	29.2	−0.80
C	trans	0.0157	40.8	4.58	7.87	11.51	3.77	3.04	4.30	28.5	−0.68
D	trans	0.0148	46.6	4.90	8.74	12.40	3.78	2.84	4.63	15.7	−0.67
E	cis	0.0951	−87.5	3.96	7.97	11.45	3.77	7.75	4.82	37.4	−0.50

[a] Dihedral angle between the linking carbonyl and the C5−C6 (alkene) bond in 1-methyl uracil. [b] Distance from the pyrenyl C1-carbon to the C5-carbon on 1-methyuracil, bridge attachment points. [c] Distance between the centers of the pyrenyl and 1-methyl uracil rings. [d] Distance between the pyrenyl C7-carbon and the N1-nitrogen on 1-methyl uracil, ring ends. [e] Lowest-energy pyrenyl singlet excited state, $(\pi,\pi^*)^1$. [f] Lowest-energy ET singlet state, $(pyrene^{\bullet+}/U_{Me}^{\bullet-})^1$. [g] For all trans conformers the uracil LUMO is the PMA-U_{Me} molecule's LUMO; however, for the cis conformer **E** the uracil LUMO is actually the molecule's LUMO + 1. Note that the pyrenyl HOMO energies are in the following ranges: −6.99 to −7.18 eV for the trans conformers and −7.14 to −7.48 eV for the cis conformers.

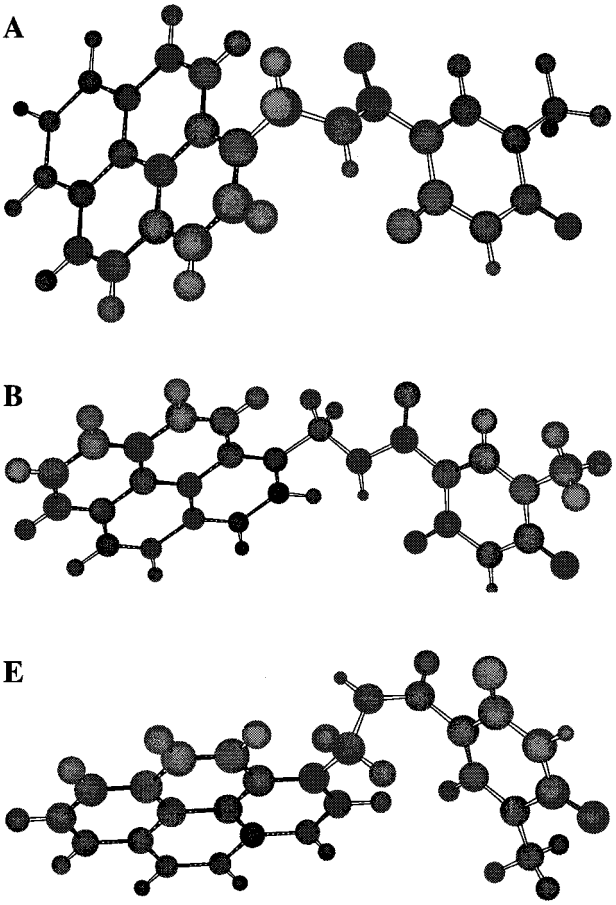

Figure 3. Three PM3 energy-minimized conformers of the PMA-U_{Me} nucleoside model. **A** and **B** have trans amide bonds, while **E** has a cis amide bond.

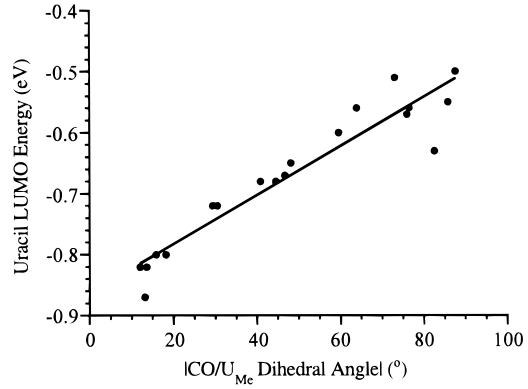

Figure 4. Linear least-squares fit of energy of the uracil LUMO in PMA-U_{Me} conformers versus the absolute value of their CO/U_{Me} dihedral angle. See Table 5 for the CO/U_{Me} dihedral angle definition. $R = 0.90$.

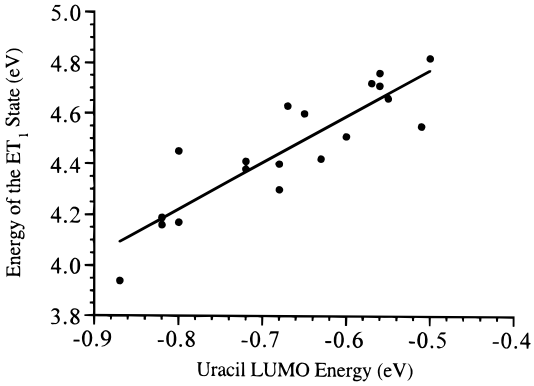

Figure 5. Linear least-squares fit of energy of the lowest-energy singlet ET (ET_1) state in PMA-U_{Me} conformers versus the energy of the uracil LUMO. $R = 0.78$.

conformers identified. The correlation coefficient R is 0.90, indicating that there is a strong correlation between the CO/U_{Me} dihedral angle and the energy of the uracil LUMO. The energy of this orbital in turn is a direct indicator of the ease of reduction of the uracil subunit. Thus, when the CO group is nearly in the plane of the C5−C6 (alkene) bond of U_{Me}, the uracil LUMO is low in energy and U_{Me} is easy to reduce.

Coulombic Effects on ET State Energies. Figure 5 is a plot of the energy of the ET_1 state versus the uracil subunit's LUMO energy in the 19 PMA-U_{Me} conformers. While there is a good correlation ($R = 0.78$) between these two parameters, this plot shows that the ET_1 energy has other contributions in addition to the location of the uracil LUMO. For example, at several uracil LUMO energies, there is a vertical spread in the ET_1 energies. Comparison of the trans conformers **A**−**D** in Table 5 gives insight into another contribution that helps determine the ET_1 state's energy.

Conformers **A** and **B** have similar CO/U_{Me} dihedral angles and uracil LUMO energies, yet they have different ET_1 energies. Comparison of the distances in Table 5 for these two conformers shows that the $pyrene^{\bullet+}$ and $U_{Me}^{\bullet-}$ subunits in conformer **B** are more widely separated than in conformer **A**. Also, conformer **B** has a higher energy ET_1 state (4.45 eV) than does conformer **A** (4.16 eV). This energy difference is consistent with less Coulombic stabilization between the cationic and anionic subunits in the ET product of conformer **B** compared to that of conformer **A**.

Three additional comparisons confirm this interpretation. First, conformers **A** and **C** have similar distances of separation between their subunits but differing CO/U_{Me} dihedral angles, 12° for **A** versus 41° for **C**. As expected from Figures 4 and 5, conformer **C** has both a higher energy uracil LUMO and a higher energy ET_1 state than does conformer **A**. Second, conformers **C** and **D** have similar CO/U_{Me} dihedral angles and similar uracil LUMO energies but differing distances of separation between their pyrenyl and uracil subunits. Again, the conformer with the greater subunit separation distance (**D**) has the higher energy ET_1 state, 4.63 eV for **D** versus 4.30 eV for **C**. Finally, conformer **D** has both a larger CO/U_{Me} dihedral angle and a greater subunit separation distance than does conformer **A**, and as expected, **D** has a substantially higher ET_1 energy (4.63 eV) than does **A** (4.16 eV). The Coulombic and CO/U_{Me} dihedral angle contributions to the energy of the ET_1 state are independent of each other and can operate either in or out of phase with respect to varying energy of the ET_1 state.

Excited-State Properties of the PMA-U_{Me} Model. The above discussion establishes two important factors that help determine the energy of the ET products in PMA-U_{Me} conformers. The first is the ease of reduction of the uracil subunit as indicated by the energy of its LUMO. The second is the amount of Coulombic stabilization between the cationic and anionic subunits in the ET product. The magnitude of the Coulombic stabilization in the gas phase is about 2 eV for cationic and anionic subunits nearly in contact versus infinitely separated. A reasonable definition of this quantity is the energy difference between the Hartree−Fock HOMO/uracil LUMO energy gap and the CIS ET_1 energy; e.g., for conformer **A** in Table 5 this is $(7.04 - 0.82) - 4.16 = 2.06$ eV.

Several other interesting observations can be made on the basis of the CIS INDO/S results for the 19 PMA-U_{Me} conformers studied. Some of these computational results for 5 conformers are given in Table 5. One is that the energies of the local pyrenyl $S_1(\pi,\pi^*)$ states are independent of conformer geometry. This is reasonable for pyrenyl and uracil subunits with weak ground-state electronic interactions. Also, the dipole moments of the $S_1(\pi,\pi^*)$ states are substantially smaller than are the dipole moments of the ET products. The dipole moment ranges of the pyrenyl $S_1(\pi,\pi^*)$ and ET_1 states for the trans conformers are, respectively, 2.5−3.9 and 11−31 D. For the cis conformers, the same ranges are, respectively, 4.4−7.7 and 22−37 D. There is no simple correlation of the ET_1 state dipole moment with any of the distance parameters listed in Table 5 that explains either the large variation of the ET_1 dipole moments or the preponderance of larger dipole moments for the cis versus the trans conformers.

INDO/S Ground-State Orbital Effects on ET_1 Product Dipole Moments. Figure 6 presents a plot of the uracil LUMO in three PMA-U_{Me} conformers, **E**, **F**, and **G**. **E** is a cis conformer and was shown previously in Figure 3. Although the CIS derived excited states do not arise solely from single HOMO to LUMO transitions, the nature and energy of the initial Hartree−Fock orbitals do exert strong effects on the final states. The effect of CO/U_{Me} dihedral angle variation on ET_1 energy is an example of this phenomenon. Conformers **E**, **F**, and **G** have ET_1 dipole moments, respectively, of 37, 19, and 11 D. Using the uracil LUMO as a measure of the spatial distribution of the highest energy electron in the $U_{Me}^{\bullet -}$ subunit suggests that the anionic charge in conformer **E** will be tightly concentrated on the C4−C5−C6 carbons and importantly will not involve the linking amide atoms or the C2 carbon. In contrast, conformers **F** and **G** (as well as all of the trans conformers) have uracil LUMO

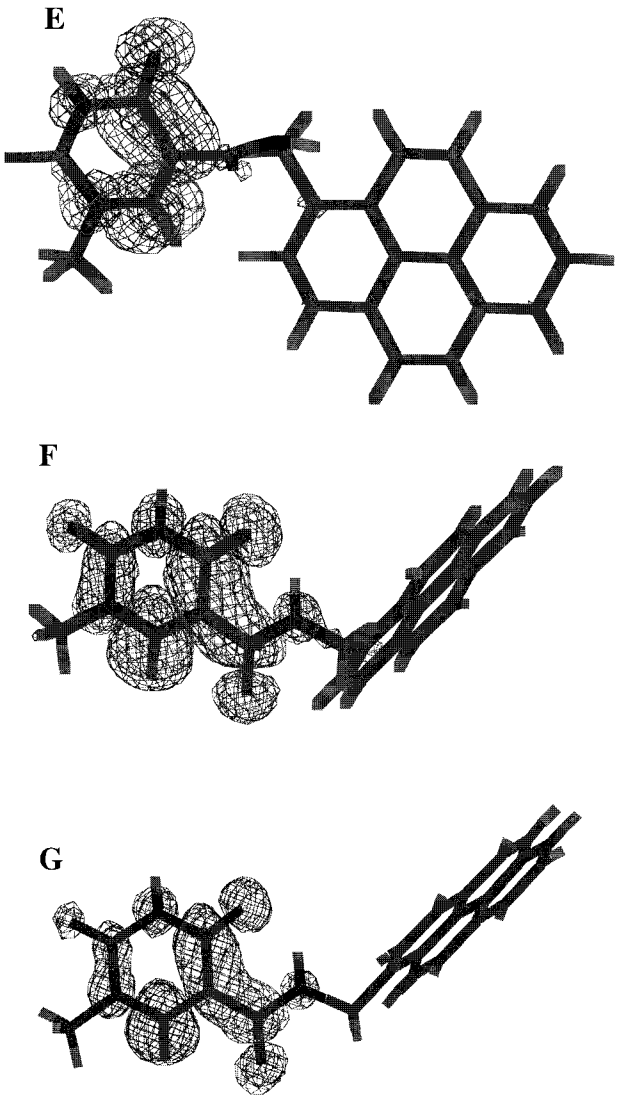

Figure 6. Plots of the uracil LUMO from INDO/S single-point calculations for three PMA-U_{Me} conformers. The LUMO representations were generated by HyperChem 5.1.

density extending well onto the amide linkage. The effect of this differential spatial distribution for the uracil LUMO is that the charge separation will be greater in cis conformers such as **E** than in trans conformers such as **F** and **G**. In general the cis conformers tend to have larger ET_1 dipole moments than do the trans conformers.

The spatial distribution of the uracil LUMO in conformers **F** and **G** can also rationalize the different sizes of their ET_1 dipole moments. In conformer **F** the uracil LUMO extends strongly onto the N1−C2−N3 atoms as well as onto the O2 atom, while in conformer **G** the uracil LUMO is concentrated on the C4−C5−C6 carbons and extends only weakly onto the N1−C2−N3 and O2 atoms. Thus, the anionic charge on the uracil subunit is shifted farther away from the cationic charge on the pyrenyl subunit in the ET_1 state of conformer **F** than it is in conformer **G**. (These charge localization arguments assume that each conformer's uracil LUMO is populated by one electron in the ET product.) The direct consequence of the greater degree of charge separation in the ET_1 state of conformer **F** is that its dipole moment (19.2 D) is larger than the corresponding dipole moment in conformer **G** (10.6 D). Remarkably, conformer **F** has a larger ET_1 state dipole moment than conformer **G**, although its C1−C5, center-to-center, and C7−N1 distances (see

Table 5 for definitions) are all 0.3−0.5 Å smaller than those in **G**. This apparent anomaly is evidence that the charge distributions in the ET_1 states of the different conformers are not uniform. The above orbital analysis of the uracil LUMOs in conformers **F** and **G** suggests that the shapes of the specific HOMOs and LUMOs involved in forming an ET_1 state have a major effect on the resulting charge distribution in this state.

Discussion and Conclusions

ET Product Lifetimes in PMA-dU. Pyrene is an attractive chromophore to attach to DNA bases for the purposes of photoreducing or photooxidizing the attached base. Pyrene has a long-lived, lowest energy $(\pi,\pi^*)^1$ excited state (219 ns for PBA and 252 ns for PMA-Ac in MeOH) and is reversibly oxidized and reduced. Thus, it offers the possibility of highly efficient charge injection or extraction from an attached DNA base.

Because the reverse ET reaction is slower than the forward one in $P_{CO}dU$ (likely by as much as a factor of 10), both reactions might be slowed in other pyrenyl-dU nucleosides by increasing the number of linking atoms to increase the lifetime of the reduced deoxyuridine species. The deoxyuridine anion could then be used for subsequent electron transfer to covalently attached electron acceptors. An additional way of increasing the lifetime of a deoxyuridine anion would be to trap it by reducing the associated pyrene cation with a nearby donor in competition with reverse ET within the pyrene$^{\bullet+}$/dU$^{\bullet-}$ product. For secondary ET trapping of dU$^{\bullet-}$ to be successful, it will likely be sufficient to slow reverse ET within the pyrenyl-dU nucleoside to the 0.5 ns range. The emission data in Table 4 at 500 nm for the PMA-dU and $P_{CO}dU$ nucleosides in MeOH show that the ET product emission is significantly longer in the former nucleoside than in the latter one. This shows that ET products live longer in the PMA-dU nucleoside than in the $P_{CO}dU$ nucleoside (respectively, 430 ps versus 67 ps for the shortest lived products in MeOH).[29] Thus, inserting the $-CH_2-NH-$ atoms between the carbonyl and pyrenyl groups in $P_{CO}dU$ to form PMA-dU slows the charge−recombination step in the latter nucleoside to the desired range.

Cis and Trans Conformers in the PMA-U_{Me} Model. For all three of the pyrenyl-dU nucleosides that have been studied to date (P-dU, $P_{CO}dU$, and PMA-dU) multiexponential $(\pi,\pi^*)^1$ emission decays were observed in all three solvents studied, THF, MeCN, and MeOH. In the cases of $P_{CO}dU$ and PMA-dU, 4 lifetimes were required to fit the emission decays in THF, and 2 or 3 were required in MeOH. In this study PM3 semiempirical conformer-search computations were performed on the PMA-U_{Me} model to learn about likely pyrenyl−uracil ground-state geometries. Then CIS INDO/S single-point excited-state computations were performed on each of the 19 conformers found in the search to learn about the energy range of their ET_1 states and about the factors that controlled this energy variation.

Semiclassical ET theory shows that ET rates depend not only on the free energy of the reaction but also on the electronic coupling and on the reorganization energy (λ) of the reaction.[39−41] While the reorganization energy for a series of PMA-dU (or PMA-U_{Me}) conformers is likely to be similar, the same may not true for their electronic coupling. We have not investigated the range of electronic coupling in the PMA-U_M conformer models, since such a study is beyond the scope of this work.

There is only indirect information concerning whether both cis and trans conformers of PMA-Ac and PMA-dU are present in this study. However, the pattern of emission decay amplitudes and lifetimes as the solvent is varied in the series THF, MeCN, and MeOH (see Table 3) does not suggest constant fractions of two different classes of conformers. Also, the energy variation of the ET_1 state within the trans family of conformers (ca. 0.7 eV) is large enough to account for the wide variation of pyrene* ET quenching (380−440 nm) and charge−recombination (500−550 nm) lifetimes. NMR evidence suggests that PMA-Ac exists only as the trans conformer. A typical barrier to rotation about the amido C−N bond is about 20 kcal/mol due to its partial double bond character.[33] Thus, cis and trans nitrogen substituents experience different chemical environments and each can usually be observed by NMR well above room temperature.[33] The ^1H spectrum of PMA-Ac shows only a single strong, sharp *N*-methyl peak; thus, it is very likely to be due to a single amide conformer. Additionally, in N-monosubstituted amides, the trans conformation is strongly preferred over the cis.[33] Importantly, in the gas and condensed phases, only the trans conformer of *N*-methylacetamide is found while in crystallographic studies both *N*-methylacetamide and *N*-phenylacetamide have the trans conformation.[33] These results imply that PMA-Ac exists solely as the trans conformer. Because steric considerations play such an important role in determining the conformation of N-monosubstituted amides, it is likely that PMA-dU exists only as the trans conformer also. In the trans geometry the N-pyrenyl and C-uracil substituents of the amido group will be farthest apart. This is similar to the situation for N-monoalkyl and C-alkyl amides where only trans conformers are found.[33]

ET Product Energies in the PMA-U_{Me} Model. The CIS INDO/S computations on the PMA-U_{Me} model show that two factors are major contributors to the variation in ET product energies among the 19 PMA-U_{Me} conformers identified. The first is the energy of the pyrenyl LUMO, and the second is the pyrenyl/U_{Me} separation distance. The energy of the pyrenyl LUMO reflects the ease of reduction of the uracil subunit with lower energies corresponding to greater ease of reduction. Clearly, making the U_{Me} subunit easier to reduce will lower the energy of a pyrene$^{\bullet+}$/$U_{Me}^{\bullet-}$ ET product. Importantly, the dihedral angle between the bridging carbonyl and the C5−C6 alkene bond in U_{Me} is strongly correlated ($R = 0.90$; see Figure 4) with the energy of the pyrenyl LUMO. This correlation is the major reason the ET product energies are higher for the cis conformers than for the trans ones; the absolute value of the CO/U_{Me} dihedral angle is 60−88° (approaching a right angle with respect to the uracil plane) for the cis conformers and 12−48° (approaching the uracil plane) for the trans ones. The second factor that contributes to the variation in ET product energies in the PMA-U_{Me} conformers is the separation distance of the cationic and anionic subunits. This is easily understood as reflecting the fact that it takes more work to separate opposite charges a larger distance than a smaller one.

Variation of either the pyrenyl LUMO's energy or the pyrene/uracil electronic coupling with conformational change is not desirable for single-step charge injection into a DNA duplex. This computational work suggests that linking pyrenyl and uracil subunits via a carbonyl attached to the uracil C5-position makes the ET product energies of such conjugates sensitive to the different relative geometries of the subunits as well as the geometries of the linking groups. Such geometry-dependent ET product energy variations should be minimized in new pyrenyl−deoxyuridine nucleosides developed for use in DNA-mediated ET studies.

Charge Recombination for PMA-dU in DNA. Charge recombination within the PMA-dU nucleoside may be both simpler and slower when incorporated into a DNA duplex than

when in solution. This may occur because the duplex structure is likely to restrict the number of closely spaced pyrenyl−uracil conformations that the PMA-dU nucleotide can adopt and favor more widely separated conformations than are typical for the PMA-dU nucleoside in solution. Also, to the extent that pyrenyl and uracil subunits are more widely separated in DNA than in solution, their ET product will be higher in energy in DNA (a Coulombic effect). Note that for this recombination reaction in a polar solvent $-\Delta G^\circ = E_{1/2}(\text{pyrene}^{\bullet+}/\text{pyrene}) - E_{1/2}(\text{d}U/\text{d}U^{\bullet-}) = 1.28 - (-1.45) = 2.73$ eV, where $E_{1/2}$ is a half-wave reduction potential (vs SCE).[42,43] Also, in polar solvents typical λ values are ca. 1.5 eV.[1,40,44−46] Thus, charge recombinations within pyrene$^{\bullet+}$/dU$^{\bullet-}$ products in polar solvents are most likely inverted reactions (where the negative of the free energy of the ET reaction, $-\Delta G^\circ$, is greater than λ).[1,39,47−49] In fact λ may be smaller in DNA than in polar solvents. Measurements of λ for ET in DNA between surface-bound and intercalated D/A groups find values of 0.66−0.70 eV.[6] Thus, charge recombination within PMA-dU in DNA will likely be even more inverted than in polar solution. Whether or not these two effects will result in a significantly slower charge recombination reaction for PMA-dU in DNA versus polar solution is an intriguing question.

Acknowledgment. This work was supported at Georgia State University and Washington State University by a Grant to T.L.N. and B.E.E. from the United States National Science Foundation (Grant No. NSF-CHE-9709318). T.L.N. thanks Marla Netzel for invaluable library research assistance.

Supporting Information Available: Figure showing ^{1}H NMR spectrum of PMA-dU. This material is available free of charge via the Internet at http://pubs.acs.org.

References and Notes

(1) Netzel, T. L. A Comparison of Theoretical and Experimental Studies of Electron Transfer Within DNA Duplexes. In *Organic and Inorganic Photochemistry*; Ramamurthy, V., Schanze, K. S., Eds.; Molecular and Supramolecular Photochemistry 2; Marcel Dekker: New York, 1998; pp 1−54.

(2) Barbara, P. F.; Olson, E. J. J. *Adv. Chem. Phys.* **1999**, *107*, 647−676.

(3) Barton, J. K. *Pure Appl. Chem.* **1998**, *70*, 873−879.

(4) Giese, B.; Wessely, S.; Spormann, M.; Lindemann, U.; Meggers, E.; Michel-Beyerle, M. E. *Angew. Chem., Int. Ed. Engl.* **1999**, *38*, 996−997.

(5) Meggers, E.; Michel-Beyerle, M. E.; Giese, B. *J. Am. Chem. Soc.* **1998**, *120*, 12950−12955.

(6) Harriman, A. *Angew. Chem., Int. Ed. Engl.* **1999**, *38*, 945−949.

(7) Fukui, K.; Tanaka, K. *Angew. Chem., Int. Ed. Engl.* **1998**, *37*, 158−161.

(8) Lewis, F. D.; Wu, T.; Zhang, Y.; Letsinger, R. L.; Greenfield, S. R.; Wasielewski, M. R. *Science* **1997**, *277*, 673−676.

(9) Ratner, M. *Nature* **1999**, *397*, 480−481.

(10) Jortner, J.; Bixon, M.; Langenbacher, T.; Michel-Beyerle, M. E. *Proc. Natl. Acad. Sci. U.S.A.* **1998**, *95*, 12759−12765.

(11) Wilson, E. K. *Chem. Eng. News* **1999**, August 23, 43−48.

(12) Kelley, S. O.; Holmlin, R. E.; Stemp, E. D. A.; Barton, J. K. *J. Am. Chem. Soc.* **1997**, *119*, 9861−9870.

(13) Kelley, S. O.; Jackson, N. M.; Hill, M. G.; Barton, J. K. *Angew. Chem., Int. Ed. Engl.* **1999**, *38*, 941−944.

(14) Kelley, S. O.; Barton, J. K. *Science* **1999**, *283*, 375−381.

(15) Wan, C.; Fiebig, T.; Kelley, S. O.; Treadway, C. R.; Barton, J. K.; Zewail, A. H. *Proc. Natl. Acad. Sci. U.S.A.* **1999**, *96*, 6014−6019.

(16) Kelley, S. O.; Barton, J. K. *Chem. Biol.* **1998**, *5*, 413−425.

(17) Stemp, E. D. A.; Arkin, M. R.; Barton, J. K. *J. Am. Chem. Soc.* **1997**, *119*, 2921−2925.

(18) Dandliker, P. J.; Holmlin, R. E.; Barton, J. K. *Science* **1997**, *275*, 1465−1468.

(19) Dandliker, P. J.; Holmlin, R. E.; Barton, J. K. *FASEB J.* **1996**, *10*, 1659−1659.

(20) Netzel, T. L. NSF Progress Report CHE-9709318, August 1998 to July 1999; National Science Foundation: Washington, DC, 1999.

(21) Netzel, T. L.; Zhao, M.; Nafisi, K.; Headrick, J.; Sigman, M. S.; Eaton, B. E. *J. Am. Chem. Soc.* **1995**, *117*, 9119−9128.

(22) Netzel, T. L.; Nafisi, K.; Headrick, J.; Eaton, B. E. *J. Phys. Chem.* **1995**, *99*, 17948−17955.

(23) Kerr, C. E.; Eaton, B. E.; Netzel, T. L. *Nucleosides Nucleotides*, **2000**, in press.

(24) Dewey, T. M.; Zyzniewski, M. C.; Eaton, B. E. *Nucleosides Nucleotides* **1996**, *15*, 1611−1617.

(25) Wahlstrom, J. L.; Ronald, R. C. *J. Org. Chem.* **1998**, *63*, 6021−6022.

(26) Lakowicz, J. R. *Principles of Fluorescence Spectroscopy*; Plenum Press: New York, 1986.

(27) Demas, J. N.; Crosby, G. A. *J. Phys. Chem.* **1971**, *75*, 991−1024.

(28) Berman, H. M.; Young, P. R. *Annu. Rev. Biophys. Bioeng.* **1981**, *10*, 87−114.

(29) Transient absorbance (TA) measurements at GSU for PMA-dU in MeOH find (1) that an expected strong absorbance increase characteristic of the pyrenyl cation is formed in ≤30 ps at 480 nm and (2) that this absorbance increase decays with the following lifetimes: 430 ± 30 ps (86% amplitude), 4.1 ns (fixed from the emission lifetime data, 6% amplitude), and longer than 10 ns (8% amplitude).[20] The slower response time of the emission detection system both overestimates the length and underestimates the amplitude of the first lifetime component compared to that of the TA system. For comparison the time resolution of the TA system is ca. 30 ps.

(30) Stewart, J. J. P. *J. Comput. Chem.* **1989**, *10*, 209−220.

(31) Stewart, J. J. P. *J. Comput. Chem.* **1989**, *10*, 221−264.

(32) *Spartan*, version 5.1.1; Wavefunction, Inc.: Irvine, CA, 1998.

(33) Robin, M. B.; Bovey, F. A.; Basch, H. Molecular and Electronic Structure of the Amide Group. In *The Chemistry of Amides*; Zabicky, J., Ed.; The Chemistry of Functional Groups; Wiley-Interscience Publishers: New York, 1970; pp 1−72.

(34) *HyperChem*, version 5.1; Hypercube, Inc.: Waterloo, Ontario, Canada, 1998.

(35) Foresman, J. B.; Head-Gordon, M.; Pople, J. A.; Frisch, M. J. *J. Phys. Chem.* **1992**, *96*, 135−149.

(36) Zerner, M. C. Semiempirical Molecular Orbital Methods. In *Reviews in Computational Chemistry II*; Libkowitz, K. B., Boyd, D. B., Eds.; VCH Publisher: New York, 1991; pp 313−366.

(37) Zerner, M. C.; Loew, G. H.; Kirchner, R. F.; Mueller-Westerhoff, U. T. *J. Am. Chem. Soc.* **1980**, *102*, 589−599.

(38) Ridley, J.; Zerner, M. C. *Theor. Chim. Acta* **1973**, *32*, 111−134.

(39) Marcus, R. A.; Sutin, N. *Biochim. Biophys. Acta* **1985**, *811*, 265−322.

(40) Brunschwig, B. S.; Ehrenson, S.; Sutin, N. *J. Phys. Chem.* **1986**, *90*, 3657−3688.

(41) Sutin, N. Nuclear and Electronic Factors in Electron Transfer: Distance Dependence of Electron-Transfer Rates. In *Electron Transfer in Inorganic, Organic, and Biological Systems*; Bolton, J. R., Mataga, N., McLendon, G., Eds.; Advances in Chemistry Series 228; American Chemical Society: Washington, DC, 1991; pp 25−43.

(42) Rehm, D.; Weller, A. *Isr. J. Chem.* **1970**, *8*, 259−271.

(43) Rehm, D.; Weller, A. *Ber. Bunsen-Ges. Phys. Chem.* **1969**, *73*, 834−839.

(44) Harriman, A.; Heitz, V.; Ebersole, M.; Vanwilligen, H. *J. Phys. Chem.* **1994**, *98*, 4982−4989.

(45) Winkler, J. R.; Gray, H. B. *Chem. Rev.* **1992**, *92*, 369−379.

(46) Cowan, J. A.; Gray, H. B. *Chem. Scr.* **1988**, *28A*, 21−26.

(47) Marcus, R. A. *J. Chem. Phys.* **1956**, *24*, 966−978.

(48) Marcus, R. A. *Science* **1992**, *256*, 1523−1524.

(49) Mines, G. A.; Ramirez, B. E.; Gray, H. B.; Winkler, J. R. *Adv. Chem. Ser.* **1998**, *254*, 51−63.